Fiber Spinning, Structure, and Properties of Poly(ethylene terephthalate-*co*-4,4′-bibenzoate) Copolyesters

Hongming Ma, Michael Hibbs, and David M. Collard

School of Chemistry and Biochemistry, Georgia Institute of Technology, Atlanta, Georgia 30332-0400

Satish Kumar*

School of Textile and Fiber Engineering, Georgia Institute of Technology, Atlanta, Georgia 30332-0295

David A. Schiraldi

KoSa, P.O. Box 5750, Spartanburg, South Carolina 29304

Received December 27, 2001; Revised Manuscript Received March 12, 2002

ABSTRACT: Thermal, rheological, and fiber spinning behavior of poly(ethylene terephthalate-*co*-4,4′-bibenzoate) random copolymers containing 5−65 mol % bibenzoate (BB) units have been studied. Copolymer randomness was determined by ^{13}C solution NMR. Copolymers with >40 mol % BB units spin like thermotropic liquid crystals and have mechanical properties approaching those of liquid crystals; however, no evidence of liquid crystallinity was observed in these fibers based on thermal, optical, and rheological studies. Thus, we believe these polymers are frustrated liquid crystalline polymers. The α-relaxation attributed to the glass transition temperature is completely suppressed in the fully drawn and heat-treated PETBB55 fibers. Structure development during fiber spinning as well as fiber mechanical properties have been studied. Fibers containing more than 40 mol % bibenzoate show the development of a new crystal structure and exhibit much higher tensile modulus than the copolymers containing a lower bibenzoate percentage. Copolymers containing more than 40 mol % bibenzoate also exhibit high melt relaxation times compared to the lower bibenzoate copolymers.

Introduction

The initial report of a thermotropic liquid crystalline polyester in 1970s by incorporation of 4-hydroxybenzoic acid (HBA) into poly(ethylene terephthalate) (PET)[1] was followed by the development of Vectra, poly(hydroxybenzoate-*co*-hydroxynaphthalate), by Celanese in 1980s.[2] The physical properties of a large number of liquid crystalline copolyesters derived from PET and a variety of dicarboxylic acids have been discussed and reviewed.[3]

The 4,4′-biphenyl moiety has been incorporated as a rigid structure unit both as diol and diacid in wholly aromatic as well as in semiflexible polyesters.[4,5] Homopolymers prepared by condensation of 4,4′-bibenzoic acid (BB) and α,ω-alkanediols, $HO(CH_2)_nOH$, in which the number of repeating methylene groups ranges from 4 to 10, are all smectic.[5−15] In contrast, low molecular weight dialkyl 4,4′-bibenzoates do not exhibit liquid crystallinity.[16]

Several papers describe the application of BB to improve the properties of PET.[3,4,17−22] Knopka reported that the modulus of a fiber spun from a 50:50 copolymer, poly(ethylene terephthalate-*co*-4,4′-bibenzoate) (PETBB50), was as high as 191 g/den (∼20 GPa).[4] Modification of PET by BB resulted in improved T_g, strength, modulus, and gas barrier properties.[20] Schiraldi et al. reported increased tensile and flexural properties and liquid-crystal-like morphology in injection-molded PETBB55 test bars.[21] Polyakova et al. reported an increase in oxygen gas barrier properties with sample orientation that is without precedent in polyester systems and again is suggestive of liquid-crystal-like behavior.[22]

High modulus in high-performance polymeric fibers is generally achieved at the expense of strain to failure. Chain folding in thermotropic polyesters and its importance in producing fibers with balanced properties (good modulus and strain to failure) have been discussed by Irwin[23] and reported a variety of copolyesters, which could be spun into high-modulus fibers also resulting in good strain to failure. In analogy to the enhanced properties of poly(ethylene naphthalate) (PEN), relative to PET, a copolymer of BB, 2,6-naphthalenedicarboxylic acid (NDA) and ethylene glycol also produces copolymer fibers with excellent tensile properties. These fibers were spun in a single spinning step, without the need for subsequent drawing or heat treatment.[24,25]

The high cost of liquid crystalline polyesters is primarily a result of the high cost of monomers (4-hydroxybenzoic acid, 6-hydroxy-2-naphthoic acid, *trans*-stilbene-4,4′-dicarboxylic acid) coupled with commercial syntheses that require in situ acylation of phenolic groups and recovery and recycling of acetic acid byproduct. An economical process for the production of 4,4′-dimethylbiphenyl and its oxidation to BB has recently been reported.[26] This provides new impetus for the careful examination of copolymers containing BB and especially its incorporation into PET under typical PET manufacturing conditions.

In this paper we report the thermal, rheological, and fiber properties of random poly(ethylene terephthalate-*co*-4,4′-bibenzoate) copolymers, PETBB, containing 5−65 mol % of the bibenzoate unit.

Experimental Section

Polymer Characterization. Poly(ethylene terephthalate-*co*-bibenzoate) (PETBB) copolymers **1** containing various amounts of bibenzoate (BB) were produced from dimethyl terephthalate, dimethyl 4,4′-bibenzoate, and ethylene glycol according to the literature method.[21] Specific polymers used

10.1021/ma012245h CCC: $22.00
Published on Web 05/11/2002

Table 1. Intrinsic Viscosities and Molecular Weights of Various Copolymers

sample[a]	IV (dL/g)	M_v (g/mol)
PET control	0.90	30 700
PETBB5	0.88	29 800
PETBB15	0.94	32 300
PETBB35	0.88	29 800
PETBB45	0.92	31 400
	1.50	56 700
PETBB55	0.81	27 000
	0.85	28 600
	0.92	31 400
	0.97	33 600
	1.20	43 400
PETBB65	0.90	30 700

[a] PETBB*x* represents poly(ethylene terephthalate-*co*-4,4′-bibenzoate) copolymer containing *x* mol % 4,4′-bibenzoate.

in this study are listed (along with their intrinsic viscosities) in Table 1. Intrinsic viscosity was measured in dichloroacetic acid solution at 25 °C.

The Mark−Houwink−Sakurada (MHS) parameters for PETBB copolymers have not been determined. The relationship between intrinsic viscosity, [η], and viscosity average molecular weight, M_v, for PET in dichloroacetic acid at 25 °C was assumed for PETBB copolymers and is given by

$$[\eta] = 1.7 \times 10^{-4}(M_v)^{0.83}$$

For comparison purposes, molecular weights of PETBB determined based on this relationship are given in Table 1.

Copolyesters were studied by ^{1}H and ^{13}C NMR spectroscopy to determine their compositions and sequences. Samples of PETBB55 and PETBB35 were dissolved in mixtures of deuterated trifluoroacetic acid (TFA-d_1) and $CDCl_3$ (approximately 5:95 v/v), and chemical shifts were measured with respect to internal tetramethylsilane (TMS). ^{1}H NMR spectra were acquired on a Bruker AMX 400 MHz instrument, and ^{13}C spectra were acquired on a Bruker DMX 500 MHz instrument using inverse gated decoupling to eliminate the nuclear Overhauser effect (NOE). A deconvolution program in the NMR software was used to integrate the ^{13}C spectra.

DSC measurements were performed on PETBB pellets on a Seiko DSC system (model 220) at a heating and cooling rate of 10 °C/min under nitrogen. Two heating and cooling cycles were employed. After the first heating the sample was held at 320 °C for 5 min to remove any thermal history. Glass transition temperature (T_g), melting temperature (T_m), and heat of fusion (ΔH_f) were recorded from the second heating curves.

Melt rheology of various PETBB copolymers was investigated using a Haake RheoStress 150 rheometer. A parallel plate sensor system with a diameter of 20 mm and gap length of 1 mm was used in conjunction with disposable aluminum pans. All samples for rheology were dried overnight at 80 °C under vacuum. Viscosity was measured as a function of shear strain rate and plotted on a log−log scale. To measure the relaxation time, the inverse of the shear strain rate at the point where polymer behavior changes from Newtonian to pseudoplastic was taken as the relaxation time for the polymer. A Leica polarized optical microscope equipped with a hot stage was used to study the morphology of PETBB polymers.

Fiber Spinning and Characterization. Fiber spinning was carried out using a piston driven small-scale fiber spinning system obtained from Bradford Research Ltd. Polymer samples were dried at ~80 °C under vacuum for 2−3 days. Fibers were spun using a single hole spinneret of 250 μm diameter. In some cases spinnerets of 500, 1000, and 2000 μm diameters were also used. Fibers were drawn on a hot plate and heat-treated at constant length in an oven.

Fiber tensile properties were measured on an Instron tensile tester (model 5567) at a gage length of 2.54 cm at a crosshead speed of 5 mm/min. Fiber diameters were measured by a laser diffraction method.[27] Twenty-five tests were conducted on each sample. The compressive strength of PETBB fiber is measured by the loop test[28,29] in an oil bath at controlled temperatures. Dynamic mechanical analysis was carried out on a Seiko DMS (model 220). A static stress of ~20 MPa and dynamic strain of 0.1% were applied for these tests using a 20 mm gauge length with approximately 20 filaments in each test. Activation energies of thermal transitions were calculated using the Arrhenius equation.[30]

Fractured fiber ends from tensile tests were sputter-coated with gold and observed by scanning electron microscopy using a Leica SteroScan 430. A Statton-Warhus camera mounted on a Rigaku generator was used to record the flat plate wide-angle X-ray diffraction patterns using Cu Kα irradiation. Kβ radiation was suppressed by a nickel filter. Interference microscopy was used to determine fiber birefringence. In our experiment a monochromatic light with a wavelength of 546 nm was used rather than a white light. For each sample, birefringence was measured on 10 samples for each fiber.

Results and Discussion

Copolymer Composition and Sequence Distribution. PETBB35 and PETBB55 are studied by ^{1}H and ^{13}C NMR spectroscopy. Conclusions as to copolymer compositions and sequence distribution are taken to be representative of all PETBB copolymers used in this study. The aromatic region of the ^{1}H spectrum of each copolymer has a multiplet at 8.14 ppm due to the bibenzoate protons (D) ortho to the ester groups. That peak is coincident with a singlet for the terephthalate proton (B). There is another multiplet at 7.72 ppm due to the bibenzoate protons meta (E) to the ester groups. Comparing the integrals of these peaks confirms that both samples have terephthalate:bibenzoate ratios that are within 1% of the ratio of monomers charged in the polymerization.

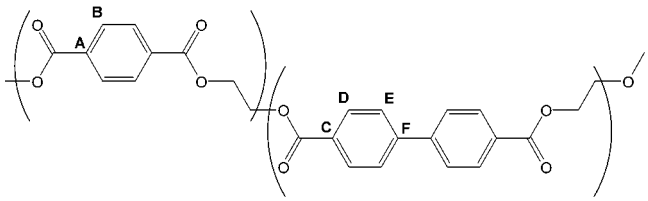

1

^{13}C NMR spectroscopy was used to determine the randomness of the sequences of the terephthalate (T) and bibenzoate (B) structural units. A similar study of poly(ethylene terephthalate-*co*-isophthalate) showed that the ipso carbons in the aryl diacids are sensitive to sequencing and could thus be used to measure the relative amounts of dyad and triad sequences.[31] The ipso carbons in the bibenzoate structural units (C) give rise to two peaks in the ^{13}C NMR spectrum of PETBB35 (Figure 1). These two peaks, at δ 128.75 and δ 128.70 ppm, can be assigned to BB and BT dyads, respectively. The ipso carbons in the terephthalate structural units (A) give rise to four peaks in the ^{13}C NMR spectrum. Two of these peaks, at δ 133.54 and δ 133.49 ppm, arise from the BTB, TTT triad sequences. The remaining two peaks at δ 133.56 and δ 133.47 ppm correspond to the BTT, TTB triad sequences, although exact assignments cannot be made. The precise value of the chemical shift of these signals is strongly dependent on the composition of the solvent. However, the ^{13}C NMR spectrum of PETBB55 displays the same six peaks due to dyad and triad sequences.

Deconvolution of the peaks and integration of the peak area allow for the determination of the relative

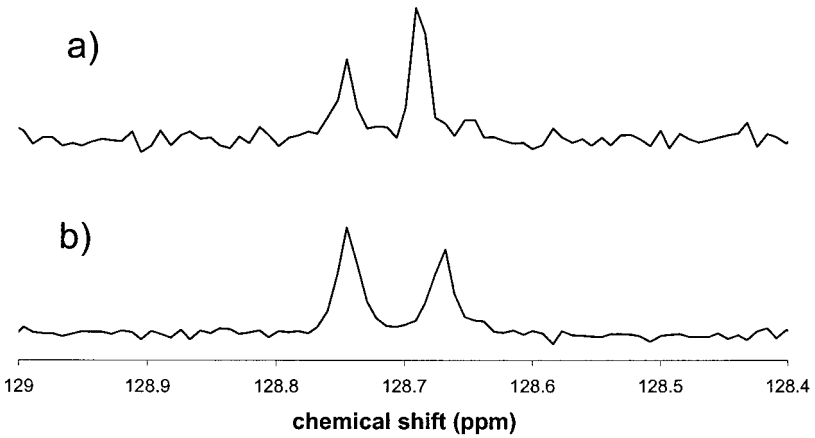

Figure 1. ^{13}C NMR spectra of (a) PETBB35 and (b) PETBB55. The peaks have been referenced to each other.

Table 2. Experimental and Theoretical (in Parentheses) Sequence Distributions for PETBB35 and PETBB55

	triads (mol %)			dyads (mol %)	
	TTT	BTT + TTB	BTB	BT	BB
PETBB35	45	44	11	63	37
	(42.25)	(45.50)	(12.25)	(65.00)	(35.00)
PETBB55	23	52	25	44	56
	(20.25)	(49.50)	(30.25)	(45.00)	(55.00)

Table 3. Thermal Transitions for PET and PETBB Copolymers

sample	T_g (°C)	T_m (°C)	ΔH_f (J/g)	T_c (°C)	$T_m - T_c$ (°C)
PET	80	252	32	184	68
PETBB5	84	240	22	163	77
PETBB15	90				
PETBB35	97				
PETBB45	102	220	14	144	76
PETBB55	103	258	17	220	38
PETBB65	110	282	39	245	37
PEBB		337,[34] 343[4]			

number of each type of diad or triad (Table 2). The experimental values, within error, match the theoretical values for the amount of each diad or triad as predicted by Bernoullian statistics for a completely random copolymer.

Thermal Analysis. Differential scanning calorimetry thermograms of unoriented polymer obtained from the polymerization are shown in Figure 2. Values of the glass transition temperature (T_g), melting point (T_m), and heat of melting (ΔH_f) from the second heating curve, and crystallization temperature (T_c) from the first cooling cycles, are compiled in Table 3.

The glass transition temperature of the copolymers increases with increasing BB mole fraction from 80 °C for pure PET to 110 °C for PETBB65 copolymer. With an increase in the mole fraction of BB, the melting temperature initially decreases, and at intermediate compositions (e.g., PETBB15 and PETBB35) the copolymers do not crystallize readily from the isotropic melt. However, at mole fraction of BB higher than about 40% crystallization takes place rapidly. The melting point and heat of melting of copolymers with greater than 40 mol % BB increase with increasing BB content. PETBB55 and -65 have higher melting points than PET homopolymer and crystallize at higher temperatures upon cooling from the melt. The less supercooling needed for crystallization as shown by $T_m - T_c$ in Table 3 indicates rapid crystallization. Thus, PETBB55 and -65 copolymers are rapidly crystallizing materials suitable for efficient use in injection molding applications.[4,21] Melting and glass transition temperatures for various PETBB copolymers are plotted in Figure 3 as a function of BB mole percentage.

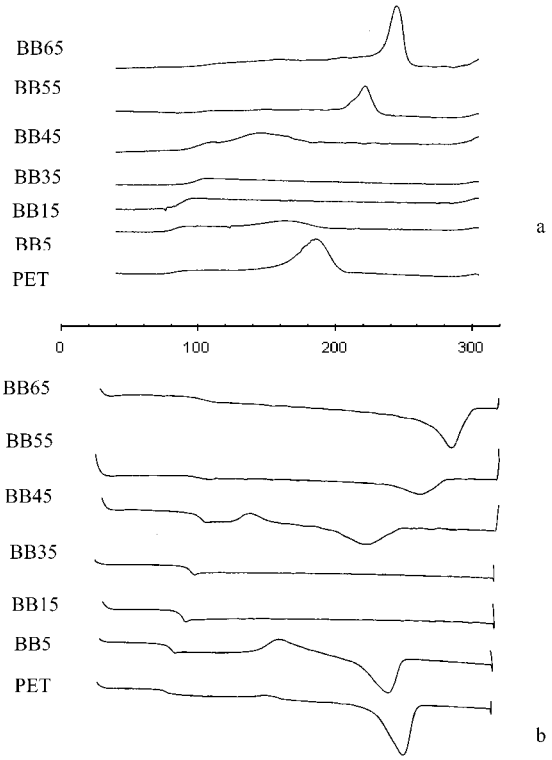

Figure 2. DSC scans of PETBBX. Heating/cooling rate 10 °C/min (a) first cooling, (b) second heating.

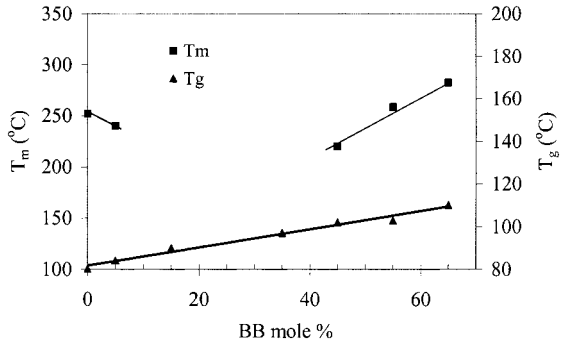

Figure 3. Melt and glass transition temperatures of unoriented PETBB copolymers (data from second heating curves).

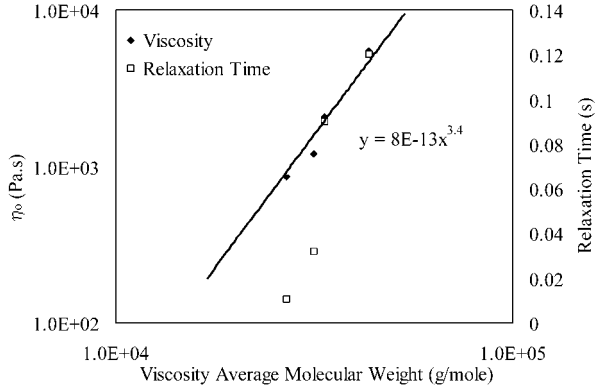

Figure 4. Melt viscosity and relaxation time as a function of viscosity-average molecular weight of PETBB55 at 300 °C.

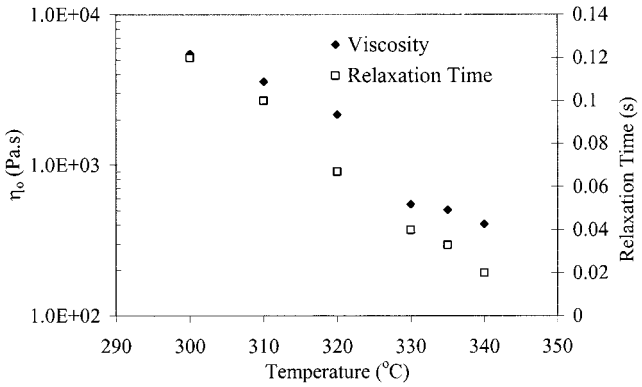

Figure 5. Melt viscosity as a function of temperature for PETBB55 (intrinsic viscosity = 1.21 dL/g).

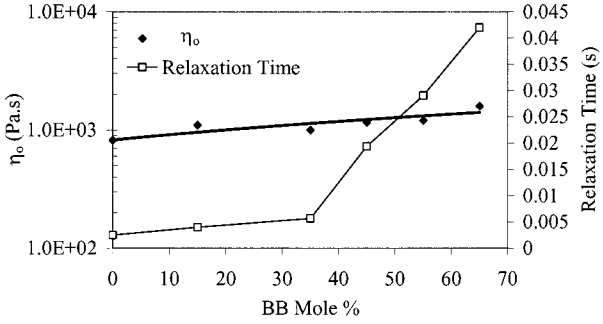

Figure 6. Melt viscosity and relaxation time for PETBB (intrinsic viscosity ~0.9 dL/g) at 300 °C as a function of BB mole content.

Rheological and Optical Behavior. As expected, zero shear viscosity and relaxation time increase with the molecular weight (Figure 4) and decrease with temperature (Figure 5). In Figure 4, the straight line is not the best fitted line; rather, it represents a slope of 3.4 for the viscosity vs molecular weight data. Zero shear viscosity and relaxation time at 300 °C are plotted as a function of BB content in Figure 6. The viscosity increases continuously with BB content. The relaxation time shows a small increase up to 40 mol % BB and then a dramatic increase for polymers containing greater than 40 mol % BB. This rapid change in relaxation time above 40% BB content coincides with the changes in crystallization behavior as well as with the development in fiber mechanical properties. As discussed later, this may suggest that at ~40% BB content the rigidity of the copolymer chain has reached a critical stage, bringing about fundamental structural changes in these copolymers, for rheology and crystallization behavior to be effected significantly. There was also a noticeable difference in the fiber spinning behavior above 40% bibenzoate content. At high BB content, fibers could be spun at high stress level (a qualitative observation) as well as have high modulus. At low BB content, the fiber threadlines tended to melt fracture when higher stresses were applied during spinning.

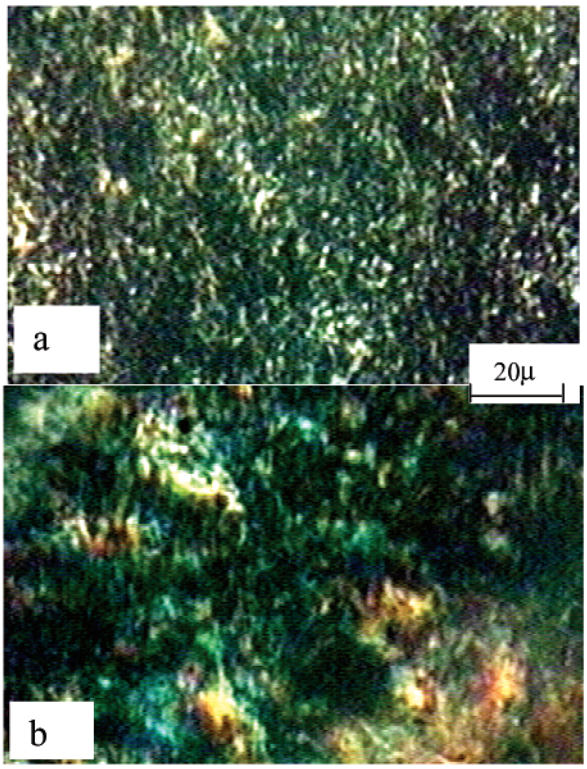

Figure 7. Optical micrographs of PETBB45 polymer cooled from isotropic melt to 210 °C, observed under cross-polars: (a) without shear; (b) slightly sheared.

The rheological behavior of PETBB copolymer is different from that of random poly(ethylene terephthalate-*co*-4-hydroxybenzoate) (PET/PHB),[3] for which the melt viscosity increases upon incorporation of hydroxybenzoate (HB) up to 30% and then decreases by an order of magnitude for polymers with greater amounts of HB. This rheological behavior was attributed to the development of liquid crystalline behavior for copolymers with greater than 30% HB. The molten state of copolymers with less than 30 mol % HB is quite transparent, whereas above this level the melt is turbid.

No evidence of liquid crystallinity has been found in PETBB copolymers.[17,21] Krigbaum et al.[17] reported that PETBB50 (IV = 0.4 dL/g) exhibited the onset of a birefringent fluid state at 204 °C upon slight depression of the coverslip, the first appearance of an anisotropic phase at 209 °C, and the disappearance of the birefringent phase at 240 °C. This sample showed one endotherm in the DSC at 203 °C; however, the authors concluded that there was no evidence of a nematic phase.

To further explore the possibility of liquid crystalline behavior in PETBB, PETBB45, -55, and -65 were examined by optical microscopy: they are birefringent up to melting temperature. Birefringence is lost above T_m, with the formation of an isotropic melt with no evidence of liquid crystallinity. On cooling from the melt, these samples exhibit a birefringent texture while the sample is still molten. Figure 7 shows the texture of

Table 4. Fiber Processing Conditions and Tensile Properties[a]

polymer	IV (dL/g)	spinning temp (°C)	draw ratio[b]	heat treatment	tensile modulus (GPa)	tensile strength (GPa)	extension to break (%)
PET	0.90	280	5	Y	10 ± 1	0.6 ± 0.1	28 ± 5
PETBB5	0.88	280	4	Y	10 ± 2	0.4 ± 0.1	22 ± 5
PETBB15	0.94	290	3	Y	8 ± 2	0.5 ± 0.1	21 ± 3
PETBB35	0.88	290−300	2	Y	15 ± 3	0.3 ± 0.1	9.0 ± 1
PETBB45	1.49	305−310	ND	N	35 ± 3	1.0 ± 0.1	4.9 ± 0.4
PETBB55	0.92	320	ND	N	32 ± 3	0.9 ± 0.1	5.1 ± 0.6
	1.2	320	ND	N	41 ± 5	1.1 ± 0.1	5.0 ± 0.7
PETBB65	0.9	310−315	ND	N	45 ± 4	0.9 ± 0.1	4.7 ± 0.6

[a] ND = not drawn, N = no heat treatment, Y = heat treated at 150 °C for 10 min. [b] Fibers drawn at 120 °C.

Table 5. Compressive Strength of PETBB55 and PET Fibers at Different Temperatures

fiber	compressive strength (GPa) at 25 (°C)	65 (°C)	105 (°C)	145 (°C)
PET	0.052 ± 0.001	0.039 ± 0.001	0.029 ± 0.001	0.009 ± 0.0003
PETBB55	0.13 ± 0.005	0.094 ± 0.004	0.053 ± 0.003	0.023 ± 0.001

supercooled PETBB45 melt at 210 °C with and without shear. This sample was heated to 320 °C and held for 5 min before cooling. Melt at this temperature was optically isotropic. The sample was allowed to cool in the hot stage and became birefringent when hot stage temperature reached 210 °C. The birefringent behavior persisted on slight shearing of the glass slide. This temperature is higher than the onset of crystallization (∼190 °C) for PETBB45 as determined by DSC curve. The presence of birefringent domains in this supercooled sample suggests that at these relatively low temperatures limited self-alignment occurs, leading to the birefringent fluidlike state. This behavior is consistent with the so-called frustrated liquid crystalline polymers.[26,32]

Fiber Spinning and Structure Development during Spinning. Conditions for fiber spinning, drawing, and heat treatment and the tensile properties of the resulting fibers are given in Table 4. At BB concentrations of less than 35 mol %, as-spun fibers exhibit poor mechanical properties, and fiber drawing and heat treatment are necessary to fully realize the properties of these fibers. The tensile moduli of the fully drawn and heat-treated fibers are comparable to those of PET homopolymer fibers. However, at greater than 40 mol % BB content, as-spun fibers have excellent tensile properties without the need of postdrawing and heat treatment steps. Much higher modulus values for PETBB fibers were obtained in this work than have been reported previously. Stress−strain curves of various PETBB copolymer fibers are given in Figure 8. For the PETBB50 copolymer fiber, Knopka[4] reported modulus values as high as ∼20 GPa (191 g/den) as compared to 41 GPa for PETBB55 obtained in this work. In addition to the tensile properties, we find that the compressive strength of PETBB55 fiber is more than twice that of PET homopolymer fiber at room temperature and at elevated temperatures. Compressive strengths of PETBB55 fiber and PET fibers at different temperatures are given in Table 5.

The effect of draw down ratio on the tensile properties and morphology of the as-spun fiber was investigated for PETBB55. Melt exit speed was controlled at 1.06 m/min. Take-up speeds up to 400 m/min were used. Wide-angle X-ray diffraction (WAXD) photographs obtained on fibers at different draw down ratios (take-up speeds/melt exit speed) are shown in Figure 9. The free fall fiber is unoriented and amorphous. Fiber orientation

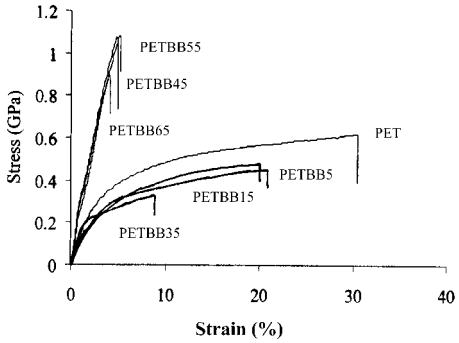

Figure 8. Typical stress−strain curves for drawn PET and PETBB fibers.

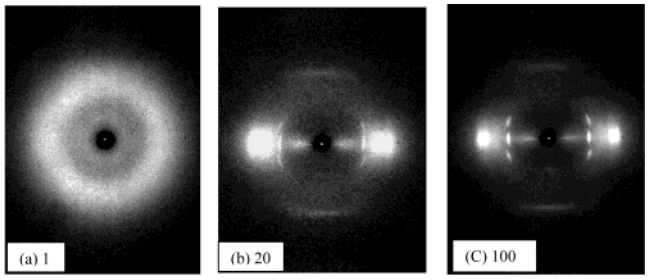

Figure 9. WAXD photographs of PETBB55 spun at 320 °C at various draw-down ratios as indicated in the photographs.

(Figure 9) and tensile modulus (Figure 10) increase dramatically with the draw down ratio and levels off at a value of about 100.

The effect of spinning temperature (280−320 °C) and spinneret size on the spinning behavior of PETBB55 was also investigated. At low temperatures, a comparatively a low draw down ratio is needed to attain the optimum tensile properties. At higher temperatures a relatively higher draw down ratio was needed to achieve similar tensile properties. No matter which spinneret was used and at what temperature, as long as the fiber was taken up at it is maximum attainable draw down ratio the tensile properties were about the same.

To study the effect of postdrawing, an unoriented amorphous PETBB55 was processed and was drawn at different temperatures to its maximum draw ratio. The unoriented amorphous nature of the fiber was confirmed by WAXD shown in Figure 11a. The maximum achievable draw ratio (this is different than the draw down ratio which was defined as the ratio of take-up speed

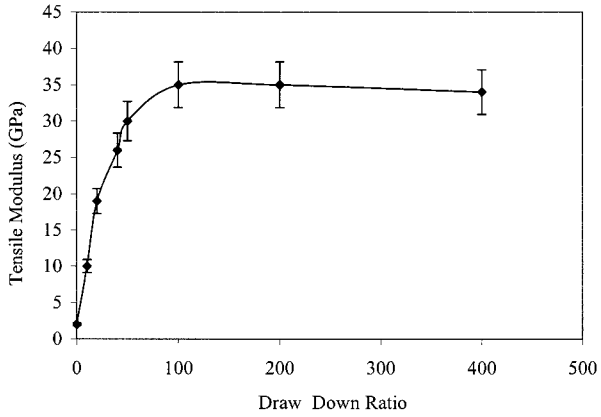

Figure 10. Tensile modulus of PETBB55 (intrinsic viscosity 0.92 dL/g) fibers obtained at different draw-down ratios.

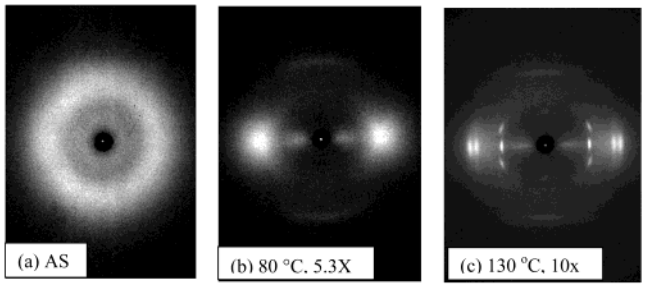

Figure 11. WAXD patterns of PETBB55 (IV = 0.81 dL/g) as-spun (AS) fiber drawn at different temperatures to the maximum attainable draw ratios as indicated.

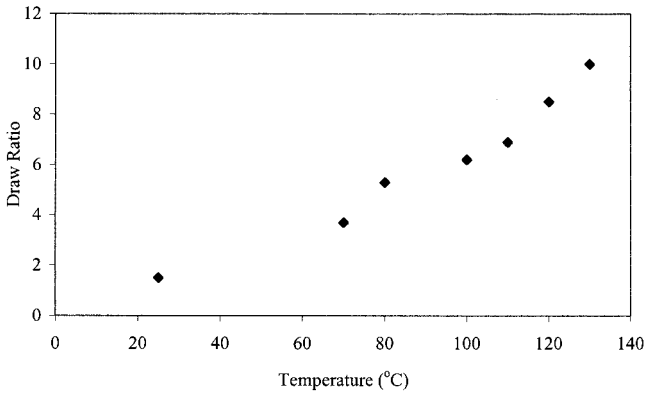

Figure 12. Maximum attainable draw ratio at different drawing temperatures for PETBB55.

to the extrusion speed) as a function of drawing temperature is plotted in Figure 12. When drawn below the glass transition temperature, only a limited draw ratio was achieved, and the fibers were oriented but amorphous (Figure 11b). However, the meridional peak in Figure 11b does suggest the presence of some axial registry. When drawn above the glass transition temperature, draw ratios as high as 10 could be achieved, and the fiber developed high crystallinity and orientation (Figure 11c). Comparison of Figure 11c and Figure 9c suggests that high orientation and crystallinity can be achieved either by a single-step take-up process at relatively high speed (as common for thermotropic liquid crystalline polymer fibers) or by a two-step process—spin at low speed followed by postdrawing and heat treatment (as common for flexible semicrystalline polymers). However, mechanical properties of the fibers processed under these two different conditions are similar.

Table 6. *d* Spacings (Å) of PET and PETBB Fibers

fibers	equatorial			off-axis
PET	5.08	3.97	3.51	5.44
PETBB5	5.09	3.98	3.50	5.45
PETBB15	5.09	3.88	3.50	5.39
PETBB35	5.08	3.93	3.46	5.46
		4.17		
PETBB45	5.62	3.70	3.47	5.23
PETBB55	5.62	3.71	3.48	5.23
PETBB65	5.62	3.69	3.46	5.24

WAXD of PET and PETBB drawn and heat-treated fibers were investigated, and the corresponding *d* spacings are listed in Table 6. At low BB concentrations (5 and 15 mol %), the observed crystal structures appeared to be identical to that of PET. However, at high BB concentrations (45−65 mol %) the fiber displayed a new set of diffractions. The PEBB homopolymer crystal structure has previously been reported[33] to be triclinic with unit cell parameters as follows: $a = 0.575$ nm, $b = 0.382$ nm, $c = 1.462$ nm, $\alpha = 90.1°$, $\beta = 90.3°$, and $\gamma = 78.1°$. However, several crystals packings including monoclinic[34] were considered possible for PETBB.[33] The reported[34] PEBB homopolymer fiber *d* spacings of 0.562, 0.371, and 0.344 nm (all equatorial) as well as off-axis spacing of 0.526 nm are close to the *d* spacings of the high BB-containing copolymers observed in this work and reported in Table 6. Comparison of these *d* spacings suggests that PETBB45 and higher BB containing copolymers have a crystal structure primarily that of the PEBB homopolymer. However, the 004 and 002 fiber diffraction peaks were reported for the PEBB homopolymer at 0.3682 and 0.7364 nm, while a meridional peak for the PETBB55 fiber (Figure 9b,c) is observed at ~0.32 nm. On the basis of the *c*-axis length of PET (1.076 nm) and PEBB (1.473 nm), a meridional spacing at 0.318 nm is predicted provided both the PET and PEBB units are randomly incorporated in the homopolymer crystal. Since the copolymer randomness has been ascertained from NMR, PETBB copolymer crystal structure appears to be that of the PEBB homopolymer in the $a-b$ plane. The *c*-axis length is based on the length of the PET and PETBB unit. Rogunova[35] investigated the morphology of melt-crystallized PETBB55 film by AFM. These AFM images show that the lamella planes of PETBB55 crystals are about 20 nm thick. The lamella thickness in PET fiber was reported to be around 10 nm, which is about 10 PET repeat units. Considering that PETBB55 is a random copolymer, this would also suggest that the crystal structure is more likely formed by cocrystallization of the two units, providing further support to the X-ray data.

Birefringence of fully drawn and crystalline PETBB55 fiber was determined to be 0.3, which is much higher than fully drawn and heat-treated PET fiber (<0.2). A scanning electron micrograph of the PETBB55 fiber cross section after tensile fracture at room temperature is shown in Figure 13. PETBB55 fibers tend to fracture in a brittle manner, with exposed "woodlike" fracture surfaces. This fracture phenomenon is comparable to the fracture of injection-molded PETBB flexural bars.[21,36]

Dynamic Mechanical Properties. The dynamic mechanical properties of drawn and heat-treated PET and PETBB fibers are compared in Figure 14. As was observed from tensile tests, the modulus of PETBB is significantly higher than that of PET. PETBB fiber also has higher modulus retention at elevated temperatures than PET. High modulus retention at elevated temper-

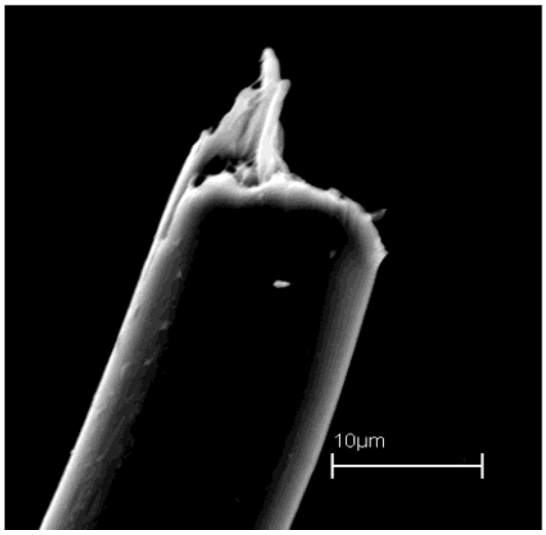

Figure 13. Tensile fracture at room temperature of PETBB55 (IV = 1.21 dL/g) tensile modulus of this fiber is ~40 GPa.

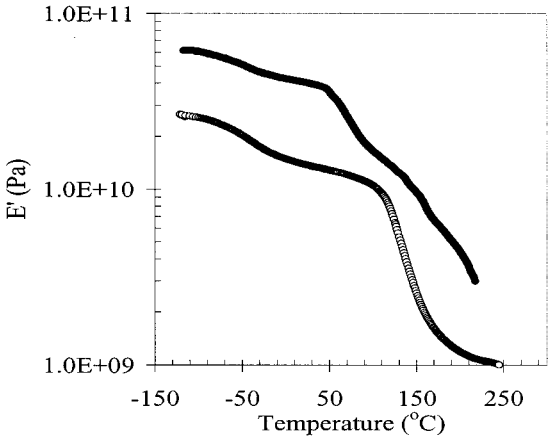

(a)

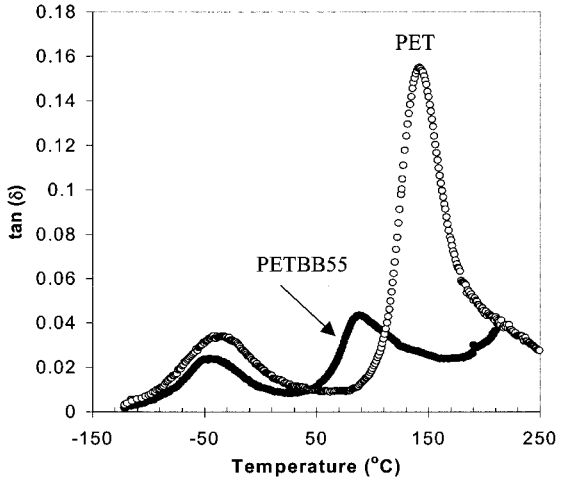

(b)

Figure 14. Dynamic mechanical properties of PET and PETBB55 fibers at 1 Hz: (a) *E′*; (b) tan *δ*.

atures is of significant importance in industrial applications such as tire sidewall reinforcement. Various transition temperatures and their activation energies in PET and PETBB55 fibers are listed in Tables 7 and 8, respectively.

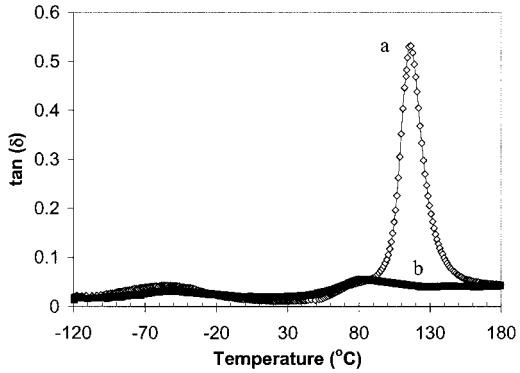

Figure 15. Tan (*δ*) as a function of temperature for PETBB55: (a) unoriented and amorphous fiber; (b) oriented and crystalline.

Table 7. Tan *δ* Peak Temperatures in PET and PETBB55 Fibers

	transition temp (°C) at 0.1, 1, and 10 Hz		
fiber	β_1	β_2	α
PET	−62, −51, −38		133, 138, 144
PETBB55	−62, −53, −43	78, 84, 89	

Table 8. Activation Energies of Various Transitions in PET and PETBB55 Fibers

	activation energy (kcal/mol)		
fiber	β_1	β_2	α
PET	18		140
PETBB55	23	105	

The *β*-relaxation in PET and PETBB55 fibers occur at the same temperature (at about −50 °C), albeit in the latter case it is of diminished magnitude. The effect of crystallinity on the *β*-relaxation of PET is small, and it has been suggested that it is a consequence of several relaxation processes, with no clear distinction between relaxation processes in the crystalline and amorphous regions.[37−42]

The glass transition peak observed at 138 °C in PET is not seen in the highly oriented and crystalline PETBB55 fiber, but a new tan *δ* peak appears at 84 °C (1 Hz) with a peak value of 0.05. The activation energy of this transition is 105 kcal/mol, lower than the activation energy for the main chain motion in the PET fibers. Asrar[20] reported two transitions in PETBB58 film at about 75 and 125 °C with peak tan *δ* values of about 0.05 and 0.3, respectively. The 125 °C transition was attributed to the main chain motion and can be termed as the α-relaxation. This relaxation appears to be completely suppressed in the highly oriented PETBB55 fiber (Figure 14). Considering that the PETBB55 fibers are highly oriented and crystalline, it is not surprising that the α-relaxation in these samples is completely suppressed. This supression of molecular relaxation is responsible for the much improved mechanical properties retention of PETBB at elevated temperatures.

To better understand the dynamic mechanical behavior of PETBB copolymer, analyses were conducted on unoriented amorphous and oriented crystalline PETBB55 fibers (Figure 15). X-ray diffraction patterns of these two fibers are represented by Figure 11a,c. Figure 15 clearly shows that the unoriented amorphous PETBB55 fiber has one α transition at 115 °C and two *β* transitions at −53 °C (β_1) and 84 °C (β_2). The two *β* transitions have comparable magnitude, though their activation energies differ significantly. We propose that

these two transitions (β_1 and β_2) involve sub-repeat unit motions containing terephthalate and bibenzoate units, respectively. As the β relaxation in PET is not significantly effected with crystallinity,[37] it appears that this relaxation in PETBB fibers is also not effected by high degree of crystallinity and order.

Conclusions

Incorporation of BB into copolymers of PET results in an increase in glass transition temperature from 80 to 110 °C for PETBB65. The copolymer melting points were depressed at low BB concentrations but increased, as expected, at high BB concentrations. At low BB content the crystal structure of PET is maintained, while at BB content above 40 mol % a new crystal structure is obtained. The structure of the new crystal in the $a-b$ plane is the same as that for the homopolymer PEBB, while the meridional spacing represents average of PET and PETBB. The melt relaxation time increased slowly at low BB mole content (<35%) but increased at much faster rate at higher BB contents. High-performance fibers of polymers containing 45−65 mol % BB are obtained in a single-step melt spinning process when melt-spun in the temperature range 290−320 °C. Without further drawing, the tensile moduli of these fibers are approximatley 40 GPa, extension to break is about 5%, and the tensile strength is about 1.0 GPa. These properties obtained without process optimization are already approaching the properties of commercially available thermotropic liquid crystalline polyesters. PETBB fibers also possess favorable mechanical properties (tensile modulus and compressive strength) retention at elevated temperatures. The α-relaxation (corresponding to a glass transition) is fully suppressed in highly oriented and crystalline PETBB55 fibers. While no evidence of liquid crystallinity in PETBB copolymers was observed from thermal, optical, and rheological methods, we believe these copolymers are frustrated liquid crystals on the basis of their processing characteristics.

Acknowledgment. This work was funded by Kosa. Fiber compressive strength was measured by M. Laton.

References and Notes

(1) Hamb, F. L. *J. Polym. Sci., Part A-1* **1972**, *10*, 3217.
(2) *Plast. World* **1985**, *43*, 65.
(3) McFarlane, F. E.; Nicely, V. A.; Davis, T. G. *Contemp. Top. Polym. Sci.* **1977**, *2*, 109.
(4) Knopka, W. N. U.S. Pat. 4,082,731, 1978.
(5) Lee, D.-K.; Tsai, H.-B. *J. Appl Polym. Sci.* **1997**, *65*, 893.
(6) Demus, D.; Richter, L. *Textures of Liquid Crystals*; Verlag Chemie: Weinheim, 1978.
(7) Watanabe, J.; Hayashi, M. *Macromolecules* **1988**, *21*, 278.
(8) Jackson, W. J., Jr.; Morrs, J. C. *Liquid Crystalline Polymers*: ACS Symposium Series 453; American Chemical Society: Washington, DC, 1990; p 16.
(9) Jackson, W. J., Jr.; Morris, J. C. U.S. Patent 4,959,450, 1988.
(10) Jackson, W. J., Jr.; Morris, J. C. U.S. Patent 5,011,878, 1990.
(11) Jackson, W. J., Jr.; Morris, J. C. U.S. Patent 5,037,946, 1990.
(12) Luyen, van D.; Strzekechi, L. *Eur. Polym. J.* **1980**, *16*, 303.
(13) Tokita, M.; Takahashi, T.; Hayashi, M.; Inomata, K.; Watanabe, J. *Macromolecules* **1996**, *29*, 1345.
(14) Tokita, M.; Osada, K.; Yamada. M.; Watanabe, J. *Macromolecules* **1998**, *31*, 8590.
(15) Osada, K.; Niwano, H.; Tokita, M.; Kawauchi, S.; Watanabe, J. *Macromolecules* **2000**, *33*, 7420.
(16) Cohen, S. D.; Risinger, C. A.; Poirier, J. C.; Swadesh, J. K. *Mol. Cryst. Liq. Cryst.* **1981**, *78*, 135.
(17) Krigbaum, W. R.; Asrar, J.; Toriumi, H.; Presston, J. *J. Polym. Sci., Polym. Lett.* **1982**, *20*, 109.
(18) Asrar, J.; Krigbaum, W. R. Preston, J.; Ciferri, A.; Toriumi, H.; Watanabe, J. *Mol. Cryst. Liq. Cryst.* **1981**, *76*, 79.
(19) Cohen, S. D.; Risinger, C. A.; Poirier, J. C.; Swadesh, J. K. *Mol. Cryst. Liq. Cryst.* **1981**, *78*, 135.
(20) Asrar, J. *Speciality Polyesters '95, Proceedings*; Schotland Business Research: Skillman, NJ, 1995; p 155.
(21) Schiraldi, D. A.; Lee, J. J.; Gould, S. A. C.; Occelli, M. L. *J. Ind. Eng. Chem.* **2000**, *7*, 67.
(22) Polyakova, A.; Liu, R. Y. F.; Schiraldi, D. A.; Hiltner, A.; Baer, E. *J. Polym. Sci., Part B: Polym. Phys.* **2001**, *39*, 1889.
(23) Irwin, R. S. *Macromolecules* **1993**, *26*, 7125.
(24) Choe, E. W.; Flint, J. A. U.S. Patent 5,453,321, 1995.
(25) Choe, E. W.; Flint, J. A. International Patent 93/02122, 1993.
(26) Sherman, S. C.; Iretskii, A. V.; White, M. G.; Schiraldi, D. A. *Chem. Innovations* **2000**, *30*, 25.
(27) Perry, A. J.; Lenichen, B.; Eliasson, B. *J. Mater. Sci.* **1974**, *9*, 1376.
(28) Sinclair, D. *J. Appl. Phys.* **1950**, *21*, 380.
(29) Kozey, V. V.; Jiang, H.; Mehta, V. R.; Kumar, S. *Mater. Res. J.* **1995**, *10*, 1044.
(30) Troughton, M. J.; Davies, G. R.; Ward, I. M. *Polymer* **1989**, *30*, 58.
(31) Martinez de Ilarduya, A.; Kint, D. P. R.; Munoz-Guerra, S. *Macromolecules* **2000**, *33*, 4596.
(32) Jung, H.-T.; Hudson, S. D.; Lenz, R. W. *Macromolecules* **1998**, *31*, 637.
(33) Wendling, J.; Gusev, A. A.; Suter, U. W.; Braam, A.; Leemans, L.; Meier, R. J.; Aerts, J.; Heuvel, J. v. d.; Hottenhuis, M. *Macromolecules* **1999**, *32*, 7866.
(34) Li, X.; Brisse, F. *Macromolecules* **1994**, *27*, 2276.
(35) Rogunova, M. *Polym. Mater. Sci. Eng.* **2001**, *84*, 435.
(36) Brown, D. M.; Clary, R. S.; Lee, C. D.; Monore, W. G.; Vaughn, D. A.; Ragheb, R. T.; Erter, J. W.; Schiraldi, D. A. *Polym. Prepr.* (*Am. Chem. Soc., Polym. Chem.*) **2000**, *41* (*1*), 123.
(37) Ward, I. M. *Mechanical Properties of Solid Polymers*; John Wiley and Sons: New York, 1979; p 180.
(38) Boyd, S. U.; Boyd, R. H. *Macromolecules* **2001**, *34*, 7219.
(39) Chen, L. P.; Yee, A. F.; Goetz, J. M.; Schaefer, J. *Macromolecules* **1998**, *31*, 5371.
(40) Maxwell, A. S.; Ward, I. M.; Laupretre, F.; Monnerie, L. *Polymer* **1998**, *39*, 6835.
(41) Wilhelm, M.; Spiess, H. W. *Macromolecules* **1996**, *29*, 1088.
(42) Gabrielse, W.; Gaur, H. A.; Feyen, F. C.; Veeman, W. S. *Macromolecules* **1994**, *27*, 5811.

MA012245H